Local Superconductivity in Vanadium Iron Arsenide

A. S. Sefat, G. D. Nguyen, D. S. Parker, M. M. Fu, Q. Zou, H. B. Cao, D. Sanjeewa, L. Li¹, Z. Gai²

We investigate the vanadium-doped iron arsenide BaFe₂As₂ in an effort to understand why Fe-site hole doping of this compound has to date never yielded bulk superconductivity. We find an (average) increase in *c*-lattice parameter of the BaFe₂As₂ lattice with the substitution of vanadium into the FeAs layers. This correlates with a lack of bulk superconductivity, as found in our previous review [1]. However, our transport and spectroscopy measurements find a coexistence of antiferromagnetic and *local* superconducting regions, observed for the first time in this in-plane hole-doped iron arsenide. In this material there is therefore a complex connection between microscopic *structural* parameters, such as composition, lattice details, doping level, and lattice strain—and the emergence of quantum states such as superconductivity and magnetism.

Materials Science & Technology Division, Oak Ridge National Laboratory, Oak Ridge, TN 37831, USA
Center for Nanophase Materials Sciences, Oak Ridge National Laboratory, Oak Ridge, TN 37831, USA
Neutron Scattering Division, Oak Ridge National Laboratory, Oak Ridge, TN 37831, USA

High-temperature superconductivity (HTS) in the iron-based materials and cuprates continues to puzzle the scientific community as its ultimate origin remains unknown despite great efforts. This is unlike the sulfur hydrides and related materials which are rather plausibly considered to be electron-phonon mediated, conventional superconductors. In these HTS, the superconducting state is typically produced by the suppression of antiferromagnetism in a parent compound through chemical substitution (x) or applied pressure. BaFe₂As₂ (referred to as '122') is an iron arsenide parent [2] with a room-temperature ThCr₂Si₂-type tetragonal crystal structure. It is itinerant and only weakly correlated with a spin-density-wave (SDW) antiferromagnetic order below Néel temperature of $T_N=133$ K, closely coupled to an orthorhombic structural transition ($T_N=T_s$). The properties of 122 can be tuned by in-plane chemical substitutions of Fe using other transition metals such as T=3d (Cr, Co, Ni, Cu), 4d (Mo, Rh, Pd, Ag), or 5d (Ir, Pt, Au) in Ba(Fe_{1-x}T_x)₂As₂ [3-12]. Previously, it was found that 3d and 4d dopants belonging to a group in the periodic table produce essentially overlapping temperature-composition (T-x) phase diagrams, emphasizing the importance of electron count [3,7,8] over lattice size effects (i.e., 3d vs. 5d). Also, it was found that d'electron' dopants (e.g., Co [5]) in 122 yield superconductivity while 'hole' dopants (e.g., Cr, Mo [3,4]) do not.

Such results are not well understood, since small doping levels of less than 5% (x<0.05) in these materials can initiate superconductivity, and it is far from clear why such small levels of disorder have such different effects when using a hole versus an electron dopant. However, first principles density-functional theory (DFT) calculations at 25% or 50% hole-dopants in 122 found a modest covalency of d with arsenic p states [4] and some dopant-induced electronic scattering [10]. A more specific experimental recipe (for any doping level) was documented in a review manuscript, finding that the c lattice parameter must shrink upon doping, to observe 'bulk' superconductivity in an in-plane doped Ba(Fe_{1-x}T_x)₂As₂ [1]. Despite all the progress in this field, it is not yet possible to predict temperature-composition (T-x) phase diagrams and the associated correlated behavior in iron arsenides. In this work, we substitute 122 with vanadium, to test whether superconductivity is induced, our idea being that vanadium is less likely to carry a large moment (compared to the other hole dopants of Mn and Cr) due to its smaller number of unpaired electrons (V³⁺, d²), and so Ba(Fe_{1-x}Vx)₂As₂ may be prone to superconductivity. While we do not find bulk superconductivity, we do find substantial evidence of local superconductivity here.

Single crystals of Ba(Fe_{1-x}V_x)₂As₂ (V-122) were grown out of FeAs self-flux technique similar to ref. [13], with [001] direction perpendicular to the plates. The chemical composition of the crystals was measured with a Hitachi S3400 scanning electron microscope energy-dispersive X-ray spectroscopy (EDS). The structures were identified as tetragonal ThCr₂Si₂ type (*I*4/*mmm*, *Z*=2) at room temperature, and lattice parameters upon doping were refined using X'Pert HighScore by collecting data on an X'Pert PRO MPD X-ray powder diffractometer (See **Table S1** in **S**upplementary section). **Fig. 1a** plots *a*- and *c*-lattice parameters as a function of V concentration. With V doping, the *a*-lattice parameter decreases while the *c*-lattice parameter increases. In the hole doped Cr-122 both *a* and *c* increase, while in Mo-122 the *a*-lattice barely changes while *c* expands. For x=0.05 in Ba(Fe_{1-x}T_x)₂As₂, the overall cell volume increases by 0.3% for T=Cr and 0.5% for Mo [3], while it only expands by ~0.1% for V. All the 122 in-plane hole-doped iron arsenides expand their *c* lattice.

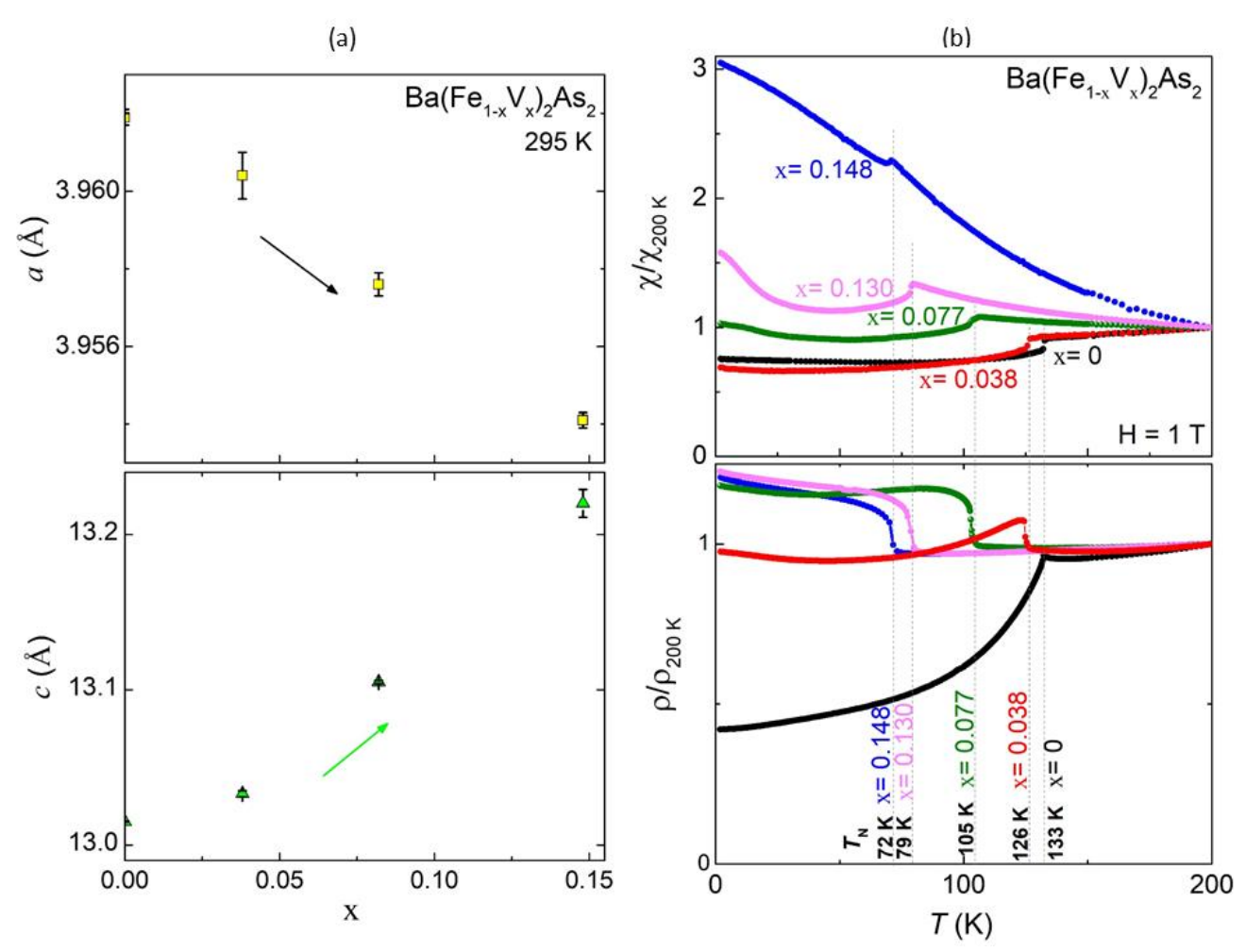


FIG. 1: Ba(Fe_{1-x}V_x)₂As₂: (a) Room-temperature tetragonal *a*- and *c*-lattice parameters for the range of possible vanadium chemical substitutions (x). (b) Temperature-dependent magnetic susceptibility χ (top) and resistivity ρ (bottom), normalized to 200 K data. Magnetization is measured in zero-field-cooling after applying 1 Tesla along *ab*-axis; resistance is measured in the *ab*-plane. Anomalies for Néel ordering temperature (T_N) match in χ and ρ . For x=0.038 T_N =128 K, and some crystals give an additional feature at T^* =20 K (see **Fig. 2a**).

Magnetization and electrical resistance data for Ba(Fe_{1-x}V_x)₂As₂ were collected using Quantum Design's magnetic and physical property measurement systems, respectively. For the temperature-sweep magnetization experiments, each sample was cooled to 1.8 K in a zero field and data were collected by warming from 1.8 to ~300 K in 1 Tesla along the *ab*-crystallographic direction. The data are presented in the form of χ/χ_{200K} for all x, to show the changes to the magnetic transitions (**Fig. 1b**, top). As expected, for the parent, χ decreases with lowering temperature and drops abruptly below T_N = T_s =133 K. For x = 0.038, 0.077, and 0.130, the χ feature persists although the transition temperatures are reduced with x; for x=0.148, the anomaly is lowest and χ increases below. The electrical resistance measurements were performed in the *ab*-plane of the crystals, by attaching platinum leads using Dupont 4929 silver paste. The values of resistivity did not change much between compositions, being on the order of a few mΩ cm, with absolute values carrying errors due to geometry factors; data is therefore presented in the form of ρ/ρ_{200K} (**Fig. 1b**, bottom). Electrical resistivity for x=0 and 0.038 diminishes with decreasing temperature, falling rapidly

below 133 K associated with T_N and T_s . The crystals with x=0.038 show an additional ρ downturn below T^* =20 K (see **Fig. 2a**), which we will discuss in detail shortly. The $\rho(T)$ for x \geq 0.077 first decreases from room temperature, and then has a sharp upturn below. This upturn in ρ reflects the loss of carriers as a partial SDW gap opens at T_N , and for temperatures below T_N , the increase in the mobility of the remaining carriers is probably not enough to overcome the lower carrier concentration and ρ continues to increase. For Ba(Fe_{1-x}V_x)₂As₂, the inferred Néel ordering temperatures estimated from the anomalies in $\chi(T)$ and $\rho(T)$ are T_N =133 K for x=0, T_N =128 K for x=0.038, T_N =105 K for x=0.077, T_N =105 K for x=0.077, T_N =79 K for x=0.130, and T_N =72 K for x=0.148. For x=0.130, neutron diffraction confirms that T_N = T_s =79 K (see **Fig. S1**) with no nematic order. Hall effect measurements indicate strong hole doping effect through V doping even at x=0.016 [14].

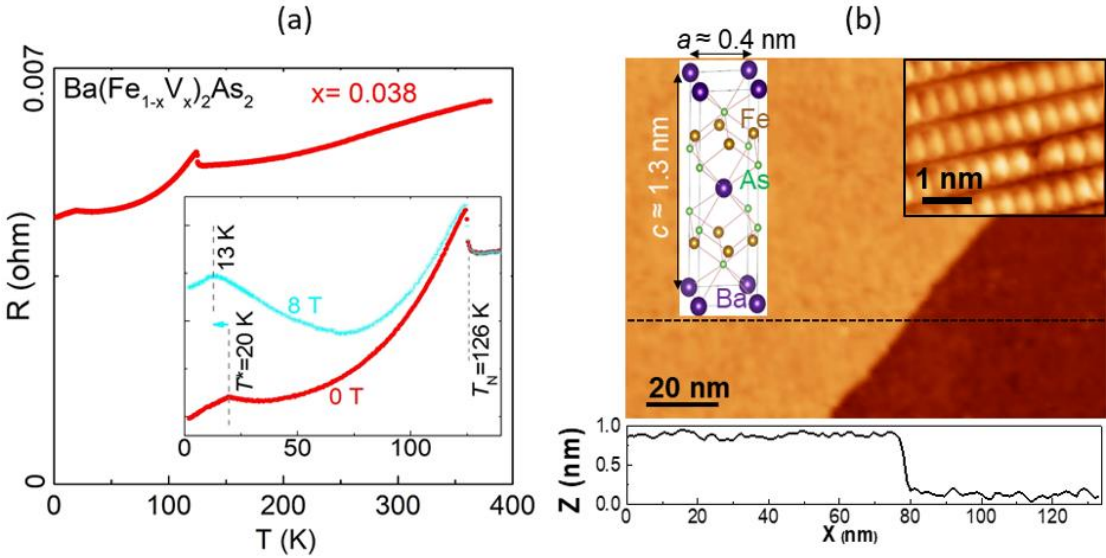


FIG. 2. For Ba(Fe_{1-x}V_x)₂As₂ crystal with x=0.038. (a) Temperature dependent resistance data on a piece, with an anomaly associated with T_N =126 K magnetic ordering, and another transition at T^* =20 K that is field dependent. (b) Large-scale STM topographic image of (V_S = -10 mV, I_t = 100 pA). Inset is a typical atomic resolution image showing 2x1 surface reconstruction (V_S = -3 mV, I_t = 200 pA).

To correlate the nanoscale structure with the bulk chemical, electronic, and magnetic behavior observed above, we performed scanning tunneling microscopy/spectroscopy (STM/S) measurement on Ba(Fe_{1-x}V_x)₂As₂ with x=0.038. The resistance data on the piece measured using STM/S is shown in **Fig. 2a**. Surprisingly, in addition to the usual anomaly at T_N , there is also a small downturn in resistance below T^* =20 K. The temperature of this downturn is reduced to 13 K upon application of an 8 Tesla magnetic field, suggestive of a superconducting state. Regarding this mysterious downturn in resistance, the literature shows other lightly hole-doped Cr [4] and Mo [3] 122 crystals having such ρ drops below T^* without reaching zero. Such a T^* transition was found to be weakly x dependent, with no structural or magnetic transitions detected via neutron scattering and was argued to result from nanoscale chemical phase segregation or perhaps an impurity inclusion [4]. Since this feature is evident in numerous lightly hole-doped crystals, we suggest that it instead has an intrinsic origin and investigate the local electronic structure for the first time here. The sample was cleaved *in situ* at liquid nitrogen temperature. A large scale STM image is shown in **Fig. 2b**, which presents large terraces and a step with a height of ~0.7 nm, close

to half the c-axis lattice parameter of 122. The inset in **Fig. 2b** shows a typical atomic resolution STM image on the surface area with 2×1 surface reconstruction.

Now we examine the electronic structure of crystal using current imaging tunneling spectroscopy (CITS) [15]. Fig. 3a presents atomically resolved STM topographic of an area. The majority of dI/dV spectra on this area show no-gap like feature as seen in **Fig. S2**. In these spectra, there is a strong nanoscale variation of spectra in this low bias range of -20 mV to +20 mV that might be due to the effect of local defects in the materials. In addition, we were also able to find some local superconducting areas in which dI/dV spectra show superconducting gap like feature. The typical dI/dV line spectra across these areas is shown in Fig. 3b (black arrow). The red curves show a superconducting-like gap with the requisite coherence peaks. In a few unit cells away, the dI/dV spectra show pseudo-gap characteristics (green curves) and then exhibit normal metallic phase behavior (black curves). Fig. 3c shows the temperature evolution of the dI/dV spectra collected on the same superconducting phase location (blue dot in Fig. 3a). With increasing temperature, this gap is suppressed and eventually disappears near 20 K. This 20 K gap suppression temperature is consistent with the downward transition temperature from our bulk resistivity measurements (Fig. 2a, inset), suggesting a common origin for these apparently distinct features. Fig. 3d plots the temperature dependence of the superconducting gap with a fitted BCS type temperature dependence [16,17].

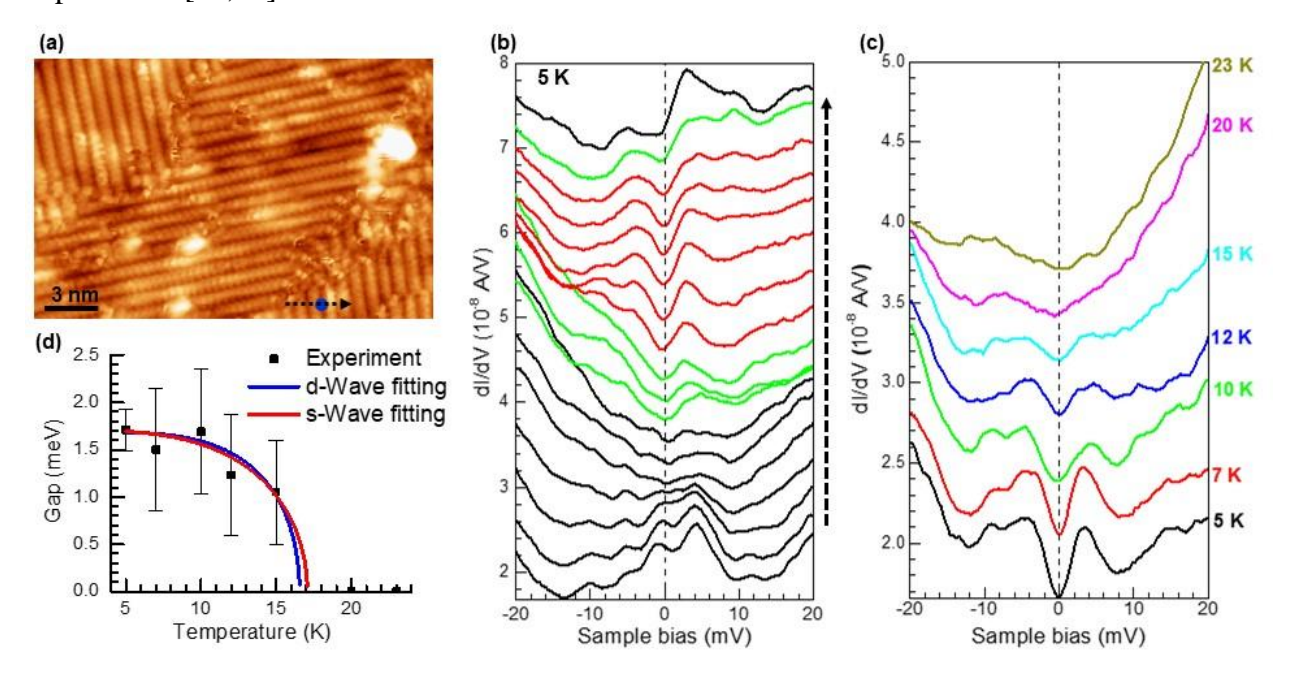


FIG. 3. (a) STM topographic image on the surface with $\mathbf{2} \times \mathbf{1}$ surface reconstruction ($V_S = -20 \text{ mV}$, $I_t = 200 \text{ pA}$). (b) $\mathrm{d}I/\mathrm{d}V$ line spectra taken across a superconducting phase area marked by the black dashed arrow in (a); spatial distance between each curve is 0.21 nm (red and green curves label the superconducting and pseudogap phase spectra, respectively). (c) Temperature dependent $\mathrm{d}I/\mathrm{d}V$ spectra taken at the same location of the blue dot in (a); vertical offsets are applied to the spectra for clarity. (d) Temperature dependence of superconducting gap with two different fittings. The gap values was averaged from 7 $\mathrm{d}I/\mathrm{d}V$ spectra data set at various superconducting positions at each temperature. A Dynes model is applied to extract the superconducting gap from $\mathrm{d}I/\mathrm{d}V$ spectra.

The superconducting gap map (Fig. 4a) at the temperature of 5 K is calculated from the CITS, similar to those reported for in-plane electron-doped iron arsenides [15]. Although the majority of the crystal shows non-superconducting behavior (zero gap), we detect small localized superconducting regions in the range of one unit-cell up to a few nanometers. The superconducting area are found mostly near domain boundaries and some bright spots on the surface which are due to sub-layer defects as seen in over layer image in Fig. 4b. In addition, we also found some surface areas of Ba(Fe_{1-x} V_x)₂As₂ crystal that show non-superconducting gap like feature in dI/dV spectra. Figs. 5a, b show an STM topographic image and dI/dV tunneling conductance map from the nonsuperconducting area. The Fast Fourier transform (FFT) of the conductance map reveals the qspace structure through quasiparticle interference (QPI) patterns induced by the scattering of electronic states with defects. The QPI disclose the C₂ symmetry of the q-space structure which is similar to QPI in the SDW state found in other iron arsenides [18]. Four white circles in Fig. 5c mark the wave vectors corresponding to the nearly square atomic lattice. There are two prominent scattering wave vectors q₁ and q₂ aligned along the Fe-Fe bond direction which is approximately 45° with the orthorhombic a- and b-axes. The scattering wave vector $q_1 \approx 2\pi/8 a_{\text{Fe-Fe}} (a_{\text{Fe-Fe}} = a_0/\sqrt{2})$ corresponds to a periodicity of $\sim 8a_{\text{Fe-Fe}}$ in real space. The wavevector q1 does not show very clearly which might be due to the scattering of the high density of defects on the sample which obscure small wave vectors. Moreoever, we observe another scattering wave vector $q_2 \approx 2\pi/4 a_{\text{Fe-Fe}}$. Based on the theoretical simulations for QPI in iron arsenides [19,20], the wave vector q₁ originates from the intrapocket scattering in a center ellipse-like hole pocket while q₂ comes from the interpocket scattering between small electron pockets beside it. Hence, non-percolative local superconductivity in the hole-doped V-122 seems to coexist with antiferromagnetism, which is evident here for the first time.

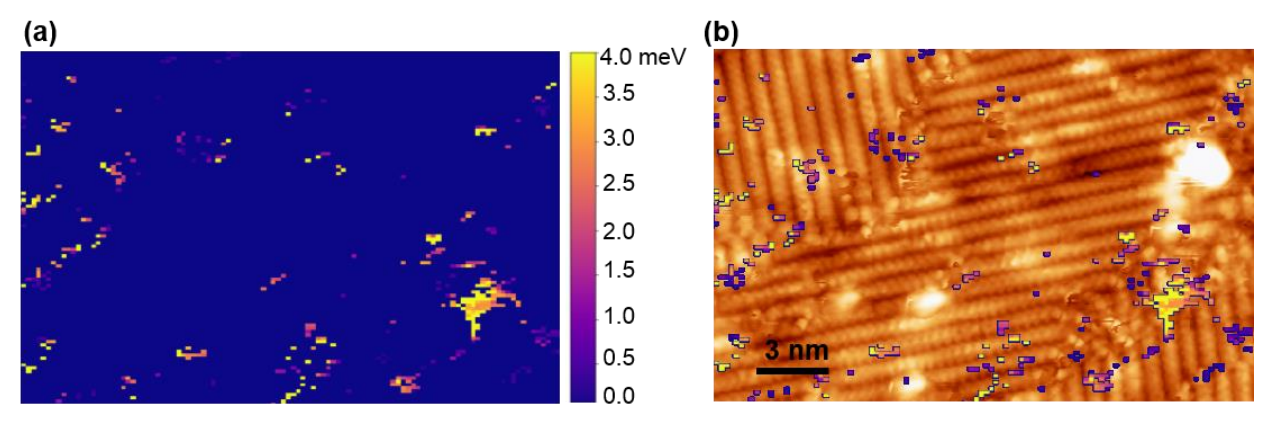


FIG. 4. (a) Superconducting gap map extracted from CITS measurement at 5 K. The gap size is calculated from coherent peak position fitting. (b) Overlay image of gap map on top of the STM image as shown in **Fig. 3a**.

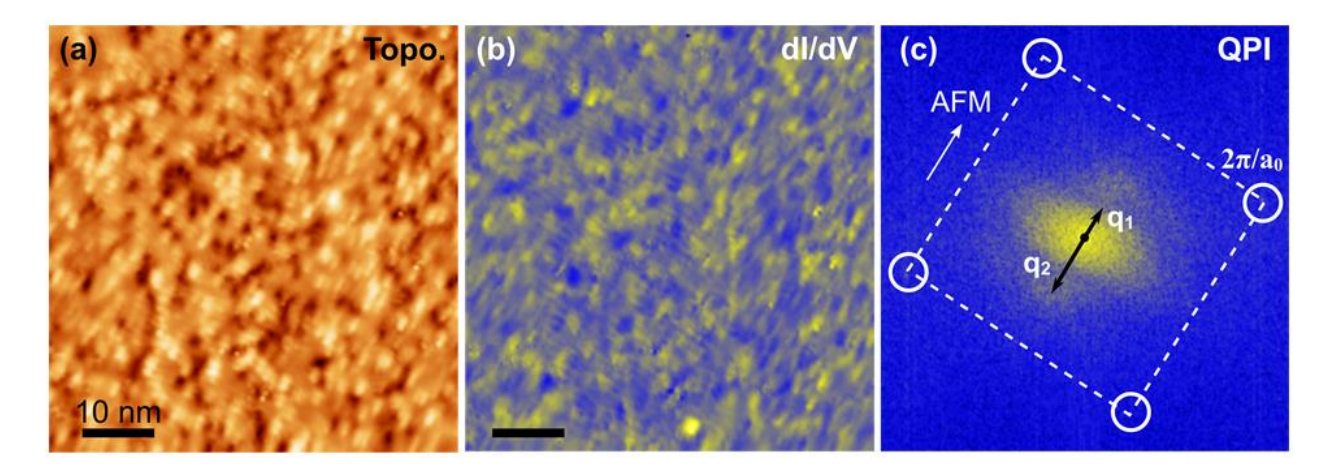


FIG 5: (a), (b) STM topographic image and dI/dV tunneling conductance map on the surface area with non-superconducting phase ($V_S = -5$ mV, $I_t = 200$ pA, $V_{ac} = 0.5$ mV, f = 973 Hz, T = 5 K). (c) FFT of conductance map in (b) which demonstrate anisotropic QPI with C₂ symmetry.

There are several other pieces of information that taken together comprise a strong case for local superconductivity in this in-plane hole-doped iron arsenide. As shown in the inset of Fig. 2a, the resistivity feature at 20 K drops to a temperature of 13 K under a field of 8 T. While it is unlikely that a spin or charge-density-wave would show such a field-related change in ordering temperature, we can even make a stronger quantitative statement. The Pauli-limited upper critical field H_{c2} , in the BCS approximation, for a 20 K superconductor would be approximately 36 T [21]. Assuming linearity in H_{c2} , one would then expect an 8 T field to reduce the resistivity feature temperature by approximately 5 K, in general agreement with the 7 K reduction we see. Moreover, there is a notable correspondence (most likely not coincidental) between these results and our previous results [5] on electron-doped BaFe₂As₂: In the work on cobalt-doped BaFe₂As₂ we observed a superconducting phase with $T_c = 21$ K for $x_{Co} = 0.1$. Note that, in terms of charge count, this is virtually an equivalent doping (of opposite sign) to our xv=0.037 doping, as V has three fewer valence electrons than Fe, and that the T_c observed there is nearly identical to our T^* here. Furthermore, in that work, we observed under application of the same 8 T field, a very similar reduction in T_c (5 K) to our 7 K reduction in T^* here. Taken together, all these facts strongly suggest that what we are observing is in fact a local superconductivity.

These local superconducting areas near domain boundaries might share the same origin as in recent proposals in iron arsenide superconductors, in which superconducting states are induced by local strains or interfaces [22-26]. In this case, however, this state is partly induced by vanadium doping. In parallel with the local superconducting phase, the crystal of $Ba(Fe_{1-x}V_x)_2As_2$ with x=0.038 also demonstrates an SDW when scanning at other crystal regions, similar to other iron arsenides [27]. Hence, this non-percolative local superconductivity in V-122 seems to coexist with antiferromagnetism. Given the likely local superconductivity around x=0.038 for V, it is plausible to argue that there is a nanoscale phase separation associated with the V substitution, with some small regions exhibiting the local superconductivity described previously and the larger fraction maintaining the antiferromagnetic character. In fact, first-principles calculations for vanadium show evidence for stronger scattering compared to cobalt dopants (see **Fig. S3**), which is likely strongest in the physical vicinity of a V dopant atom and weaker at a greater distance. As the

doping level is rather low (<4%), this may yield variation in bulk ρ properties in different pieces of as-grown crystals.

We note that this apparent local superconductivity only appears at (and presumably near) the low doping of x=0.038. For samples with larger doping levels there is no hint of the several superconductivity-related features descried above. It is most likely that this is related to the substantial scattering the V dopant atoms produce, as shown in our first principles calculations in Fig. S3. In general, superconductivity in these materials results from a complex constellation of effects – the role of charge doping in suppressing the magnetic order, changes in unit cell parameters, local strain, the strength of spin fluctuations, and the pair-breaking effects of the scattering due to the dopant atom. It is still an open theoretical question, for example, why doping the usually strongly magnetic Co atom into BaFe₂As₂ in fact *suppresses* the magnetic order and leads to robust superconductivity.

We also note that there is an experimental precedent in BaFe₂As₂ for this highly doping-dependent superconductivity. Unlike Co and Ni doping, which both produce a strong superconductivity with T_c values exceeding 20 K, Cu doping [28] produces only a minimal ($T_c \sim 2$ K) superconductivity at the very small doping (quite similar in charge count to x=0.038 of V here) of x=0.044. We have previously argued [9] that this results from strong scattering associated with the Cu atoms, which effectively form a rather distinct band associated with large pair-breaking. While the scattering due to V is somewhat weaker than in Cu, the same effect is generally operative here, with the additional distinction that for this small V doping the magnetic state is not fully suppressed. This is most likely due to the unfilled d-shell of V, and therefore the magnetism probably interacts with the local superconductivity in some manner. Future theoretical and experimental work is necessary to understand this relationship. We also note that, most likely due to a solubility limit, we have not synthesized samples with x > 0.147, so that potential superconducting behavior in this regime remains unexplored.

A major unanswered question is the local relationship of the vanadium with the apparent superconductivity. It is tempting to associate the few percent reductions in ρ in the superconducting phase with the few percent (x=0.038) of V present in the crystal and thereby correlate the location of the V atom with the local superconductivity. However, the STM results do not confirm this and in addition, in such a scenario the local environment would be very highly doped, containing an electron count (per cell) of order unity less than the majority phase. This is unlikely to show superconductivity with the $T^*c\sim20$ K that we observe. It is more likely that a combination of charge doping, strain, and reduced scattering in the vicinity of the grain boundaries allows local superconductivity to emerge in this in-plane hole-doped iron arsenide.

To summarize, we find substantial evidence of novel local superconductivity in vanadium-doped BaFe₂As₂ crystals, which appears to coexist, in a phase-separated manner, with antiferromagnetism. Such *local* superconductivity in an iron arsenide, along with coexisting magnetism is consistent with the *lack* of bulk superconductivity at higher x for any in-plane hole-dopants (e.g., V, Cr, Mo, Mn) and yields additional questions regarding the possibility of a percolative superconducting path in these materials.

Acknowledgement

This manuscript has been authored by UT-Battelle, LLC under Contract No. DE-AC05-00OR22725 with the U.S. Department of Energy. The United States Government retains and the publisher, by accepting the article for publication, acknowledges that the United States Government retains a non-exclusive, paid-up, irrevocable, world-wide license to publish or reproduce the published form of this manuscript, or allow others to do so, for United States Government purposes. The Department of Energy will provide public access to these results of federally sponsored research in accordance with the DOE Public Access Plan.

The research is supported by the U.S. Department of Energy (DOE), Office of Science, Basic Energy Sciences (BES), Materials Science and Engineering Division. STM/S study was conducted at the Center for Nanophase Materials Sciences, which is a DOE Office of Science User Facility. This research used resources at the High Flux Isotope Reactor, a DOE Office of Science User Facility operated by the Oak Ridge National Laboratory.

References

- [1] L. M. N. Konzen, and A. S. Sefat, J. Phys.: Condens. Matter **29** (2017), 083001.
- [2] M. Rotter, M. Tegel, D. Johrendt, I. Schellenberg, W. Hermes, and R. Pottgen, Phys. Rev. B 78, 020503 (2008).
- [3] A. S. Sefat, K. Marty, A. D. Christianson, B. Saparov, M. A. McGuire, M. D. Lumsden, W. Tian, and B. C. Sales, Phys. Rev. B 85, 024503 (2012).
- [4] A. S. Sefat, D. J. Singh, L. H. VanBebber, Y. Mozharivskyj, M. A. McGuire, R. Jin, B. C. Sales, V. Keppens, and D. Mandrus, Phys. Rev. B **79**, 224524 (2009).
- [5] A. S. Sefat, R. Jin, M. A. McGuire, B. C. Sales, D. J. Singh, and D. Mandrus, Phys. Rev. Lett. **101**, 117004 (2008).
- [6] N. Ni, and S. L Bud'ko, Mater. Research Bull. 36, 620 (2011).
- [7] K. Marty, A. D. Christianson, C. H. Wang, M. Matsuda, H. Cao, L. H. VanBebber, J. L. Zarestky, D. J. Singh, A. S. Sefat, and M. D. Lumsden, Phys. Rev. B 83, 060509(R) (2011).
- [8] N. Ni, A. Thaler, A. Kracher, J. Q. Yan, S. L Bud'ko, and P. C. Canfield, Phys. Rev. B **80**, 024511 (2009).
- [9] L. Li, H. Cao, D. S. Parker, S. J. Kuhn, and A. S. Sefat, Phys. Rev. B 94, 134510 (2016).
- [10] X. Zhu, F. Han, G. Mu, P. Cheng, J. Tang, J. Ju, K. Tanigaki, and H.-H. Wen, Phys. Rev. B **81**, 104525 (2010).
- [11] X. L. Wang, H. Y. Shi, X. W. Yan, Y. C. Yuan, Z.-Y. Lu, X. Q. Wang, and T.-S. Zhao, Appl. Phys. Lett. **96**, 12507 (2010).
- [12] L. Li, H. Cao, M. A. McGuire, J. S. Kim, G.R. Stewart, and A. S. Sefat, Phys. Rev. B **92**, 094504 (2015).
- [13] A. S. Sefat, Current Opinion Solid State Mater. Sci. 17, 59 (2013).
- [14] new paper
- [15] Q. Zou, Z. M. Wu, M. M. Fu, C. M. Zhang, S. Rajput, Y. P. Wu, L. Li, D. S. Parker, J. Kang, A. S. Sefat, and Z. Gai, Nano Lett. **17**, 1642 (2017).
- [16] C. Poole, R. Prosorov, H. A. Farah, R. J. Creswick, Superconductivity 3rd Ed. 445 (2014).
- [17] K. Senapati, M. G. Blamire, Z. H. Barber, Nature Mater. 10, 849 (2011).
- [18] H. Xiao, T. Hu, A.P. Dioguardi, N. Roberts-Warren, A.C. Shockley, J. Crocker, D.M. Nisson, Z. Viskadourakis, X. Tee, I. Radulov, C. C. Almasan, N. J. Curro, and C. Panagopoulos, Phys. Rev. B **85**, 024530 (2012).

- [19] J. Knolle, I. Eremin, A. Akbari, and R. Moessner, Phys. Rev. Lett. **104**, 257001 (2010).
- [20] D. K. Singh, and P. Majumdar, Phys. Rev. B **96**, 235111 (2017).
- [21] S. Khim, J. W. Kim, E. S. Choi, Y. Bang, M. Nohara, H. Takagi, and K. H. Kim. *Phys. Rev. B* 81, 184511 (2010).
- [22] S. Saha, N. Butch, K. Kirshenbaum, J. Paglione, and P. Zavalij, Phys. Rev. Lett. **103**, 037005 (2009)
- [23] K. Zhao, B. Lv, L. Deng, S.-Y. Huyan, Y.-Y. Xue, and C.-W. Chu, Proc. Natl. Acad. Sci. 113, 12968 (2016).
- [24] J. Engelmann, V. Grinenko, P. Chekhonin, W. Skrotzki, D.V. Efremov, S. Oswald, K. Iida, R. Hühne, J. Hänisch, M. Hoffmann, F. Kurth, L. Schultz, and B. Holzapfel, Nature Comm. **4**, 2877 (2013).
- [25] H. Xiao, T. Hu, A.P. Dioguardi, N. Roberts-Warren, A.C. Shockley, J. Crocker, D.M. Nisson, Z. Viskadourakis, X. Tee, I. Radulov, C. C. Almasan, N. J. Curro, and C. Panagopoulos, Phys. Rev. B **85**, 024530 (2012).
- [26] T. Ozaki, L. Wu, C. Zhang, J. Jaroszynski, W. Si, J. Zhou, Y. Zhu, and Q. Li, Nature Comm. 7, 13036 (2016).
- [27] J. E. Hoffman, Rep. Prog. Phys. **74**, 124513 (2011).
- [28] N. Ni, A. Thaler, J. Q. Yan, A. Kracher, E. Colombier, S. L. Bud'ko, P. C. Canfield, and S. T. Hannahs. Phys. Rev. B **82**, 024519 (2010).

Supplemental Material for

Local Superconductivity in Vanadium Iron Arsenide

A. S. Sefat, G. D. Nguyen, D. S. Parker, M. M. Fu, Q. Zou, H. B. Cao, D. Sanjeewa, L. Li, Z. Gai²

In this Supplement, we provide additional information regarding: (i) growth and structure, (ii) local magnetic structure, (iii) density of states.

GROWTH AND STRUCTURE

To produce a range of dopant concentrations of Ba(Fe_{1-x}V_x)₂As₂ crystals, small barium chunks, V powder (VAs powder for getting uniform sample with high doping level), and FeAs powder were combined according to various loading ratios of V(or VAs): FeAs in alumina crucibles. A second catch crucible containing quartz wool was placed on top of each growth alumina crucible, and both were sealed inside a silica tube under ~1/3 atm argon gas. Each reaction was heated for ~24 h at 1180 °C, and then cooled at a rate of 2°C/h, followed by a decanting of the flux around 1090 °C [S1]. The several-millimeter sized crystals formed with the [001] direction perpendicular to the plates. The chemical composition of the crystals was measured with a Hitachi S3400 scanning electron microscope operating at 20 kV and use of energy-dispersive x-ray spectroscopy (EDS). For finding the level of x, at least three spots (~90 µm diameter each) were averaged on crystalline pieces in each as-grown batch. The measured EDS values are reported as vanadium (x) in Table S1, and thermodynamic and transport bulk properties are denoted by x. Phase purity and lattice parameters upon doping were checked by collecting data on an X'Pert PRO MPD X-ray powder diffractometer in the 5–90° 2θ range. At room temperature, the structures were identified as the tetragonal ThCr₂Si₂ structure type (I4/mmm, Z=2). The air and moisture stability of the crystals were confirmed by rechecking the diffraction scan of a sample left overnight. Lattice parameters were determined from full-pattern LeBail refinements using X'Pert HighScore, listed in **Table S1**.

Single crystal neutron diffraction was performed at the High Flux Isotope Reactor at ORNL, using HB-3A four-circle neutron diffractometer, on a crystal of Ba(Fe_{1-x}V_x)₂As₂ with x=0.130 in order to confirm magnetism and coupling of magnetic and structural transitions inferred from properties at ~79 K. Results are shown in **Fig. S1**, also featuring data of the parent as comparison. The ordering temperature for the magnetic transition from paramagnetic state to SDW order [122 with known propagation vector in Tetragonal cell (½ ½ 1)_T or in orthorhombic cell (1 0 1)₀] is determined by the intensity of the magnetic reflection (½ ½ 5)_T/(1 0 5)_O. For tracking the tetragonal-to-orthorhombic transition, the intensity of the (2 2 0)_T nuclear peak was measured with warming; the intensity increase below the T_s is due to a reduced extinction effect, caused by the structural transition from tetragonal to split into (4 0 0)_O and (0 4 0)_O reflections (O refers to orthorhombic vector basis), resulting in a significant change in the peak intensity at the transition. Hence for x=0.130, neutron diffraction confirms that T_N = T_s =79 K.

Materials Science & Technology Division, Oak Ridge National Laboratory, Oak Ridge, TN 37831, USA
Center for Nanophase Materials Sciences, Oak Ridge National Laboratory, Oak Ridge, TN 37831, USA
Neutron Scattering Division, Oak Ridge National Laboratory, Oak Ridge, TN 37831, USA

The local electronic structure of crystal of Ba(Fe_{1-x}V_x)₂As₂ crystal with x=0.038 using current imaging tunneling spectroscopy is presented in **Fig. S2**, showing atomically resolved STM topographic of an area. The majority of dI/dV spectra on this area show no-gap like feature.

TABLE S1. A few of flux grown $Ba(Fe_{1-x}V_x)_2As_2$ crystals: the resulting vanadium concentration (x) and the refined lattice parameters.

V (x)	<i>a</i> -lattice parameter (Å)	c-lattice parameter (Å)
0	3.9619(2)	13.0151(2)
0.038	3.9604(6)	13.033(2)
0.082	3.9576(3)	13.105(1)
0.148	3.9541(2)	13.220(9)

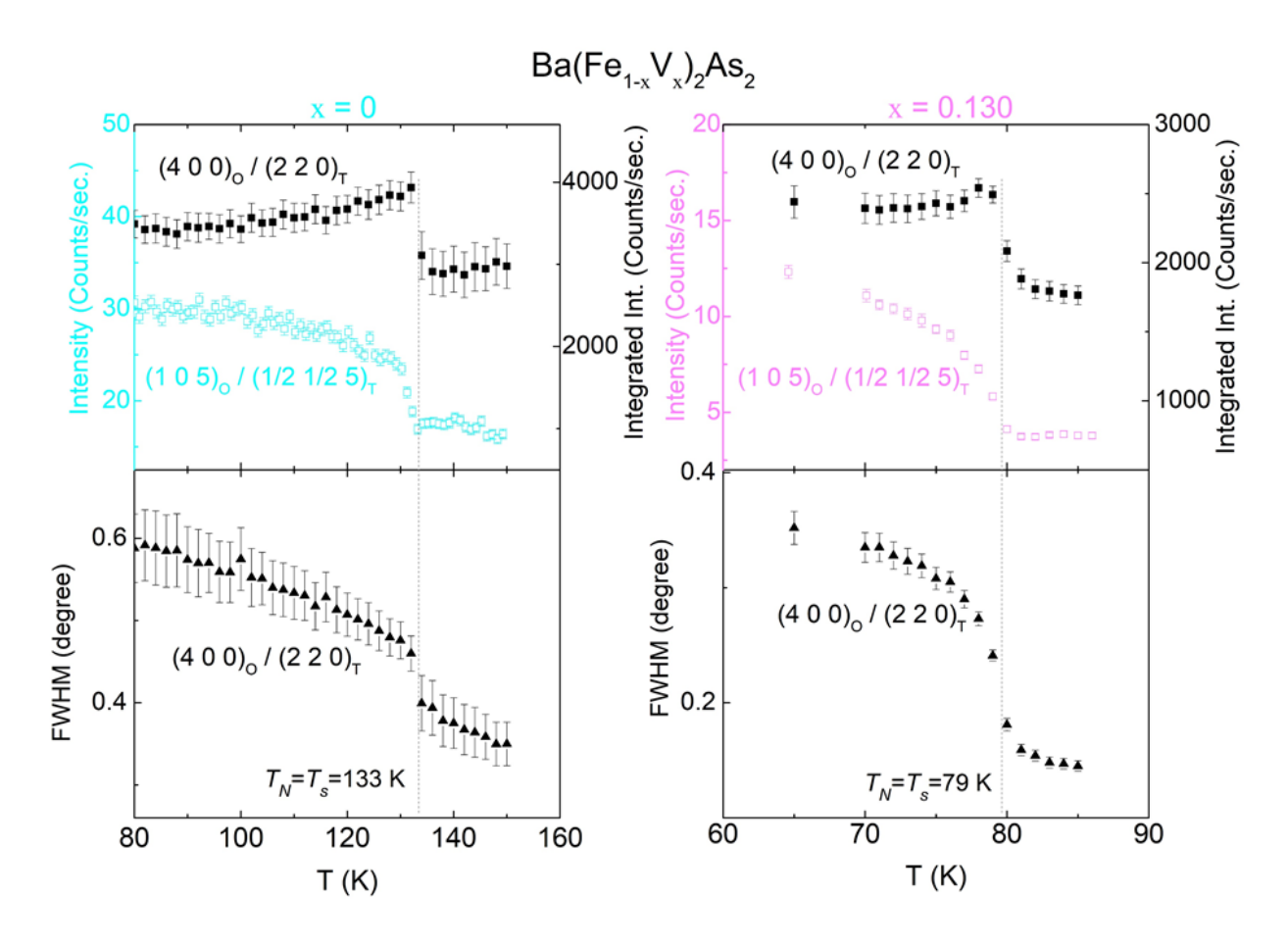


FIGURE S1. For Ba(Fe_{1-x}V_x)₂As₂ crystals, neutron diffraction results for x=0 (left) compared to x=0.130 (right). Top panels: integrated intensity of the nuclear peak (4 0 0)_O/(2 2 0)_T and peak intensity of magnetic peak (1 0 5)_O/(½ ½ 5)_T. Bottom panels: full width at half maximum values of peaks. The dashed lines mark the overlapped structural and magnetic transition for both samples at T_N = T_s .

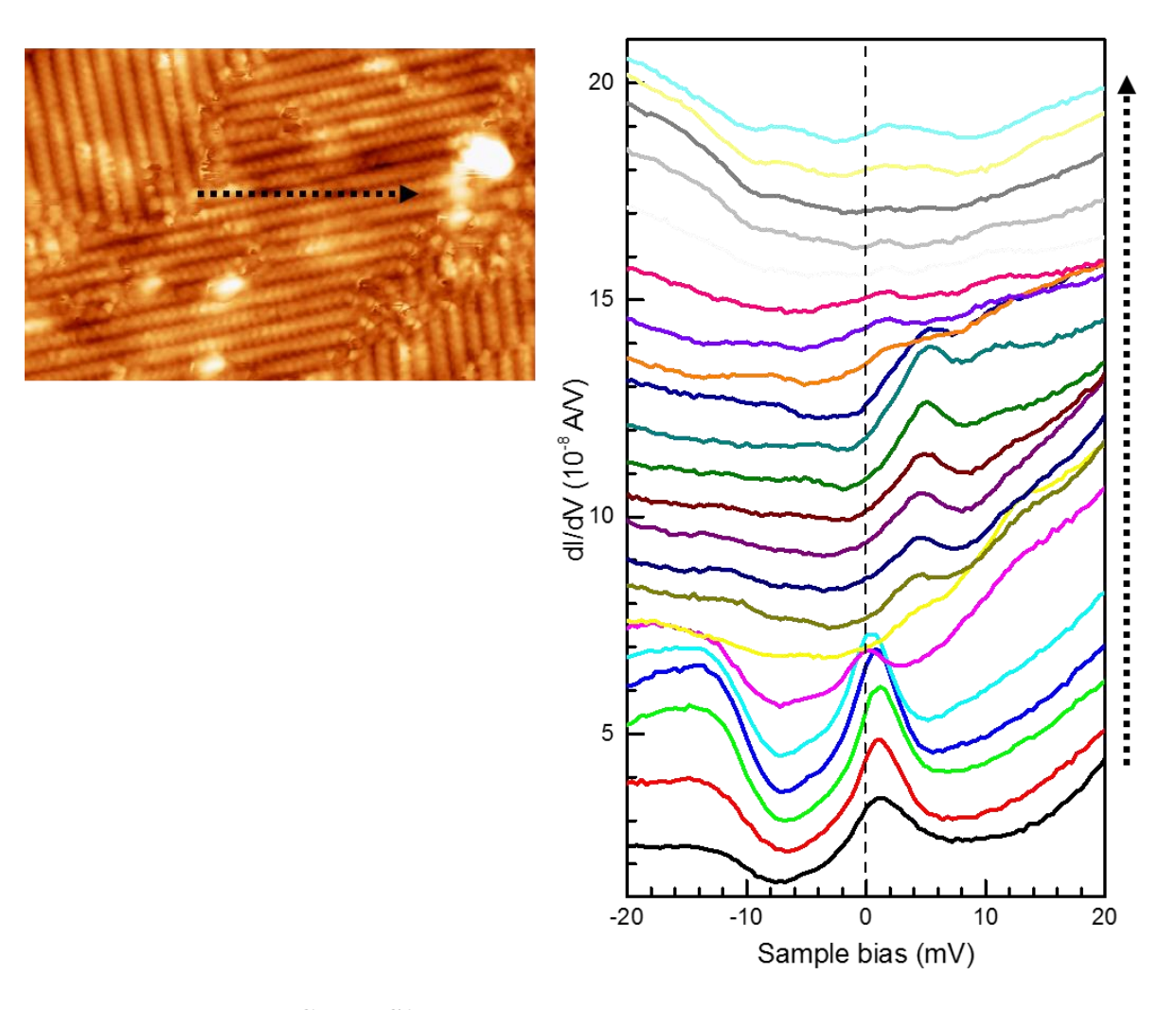


FIGURE S2:Line spectra on a non-superconducting region.

DENSITY OF STATES

The DOS for cobalt versus vanadium dopants into BaFe₂As₂ are shown in **Fig. S3**. These calculations were performed using the orthorhombic lattice parameters for 122, with one of the eight Fe substituted by the respective dopant, in a non-magnetic state. As before, we use the local density approximation and experimental arsenic height in these calculations [S2-S4]. Comparing cobalt to vanadium, cobalt is suggested for robust superconductivity as its DOS mimics that of the overall crystal matrix, both in shape and proportion, resulting in minimal scattering for substituting in 122. For vanadium, there is an absolute maximum approximately 1 eV above E_F and some 1 to 2 eV above the corresponding maxima in the total DOS curve. This difference in shape indicates the likelihood of significant additional scattering compared to that of Co, but not as extreme as in Ag doping [S2]. Speaking from a real-space perspective, such scattering is likely stronger in the physical vicinity of a V dopant atom and would be expected to be weaker at a greater distance.

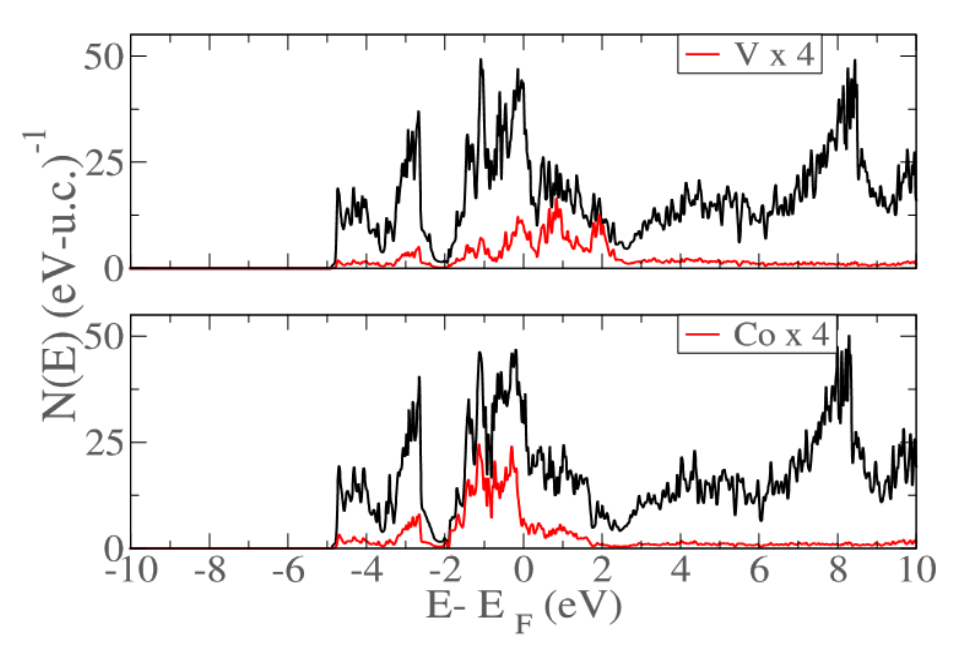


FIGURE S3. Calculated DOS for cobalt versus vanadium dopants into BaFe₂As₂. The DOS of the dopants is multiplied by 4 for clarity.

[S1] A. S. Sefat, Current Opinion Solid State Mater. Sci. 17, 59 (2013).

[S2] L. Li, H. Cao, D. S. Parker, S. J. Kuhn, and A. S. Sefat, Phys. Rev. B 94, 134510 (2016).

[S3] A. S. Sefat, L. Li, H. Cao, M. A. McGuire, B. C. Sales, R. Custelcean, and D. S. Parker, Sci. Rep. 6, 21660 (2016).

[S4] I. I. Mazin, M. D. Johannes, L. Boeri, K. Koepernik, and D. J. Singh, Phys. Rev. B **78**, 085104 (2008).